Journal of Southeast University (English Edition) Vol. 40, No. 2, pp. 165 - 175 June 2024 ISSN 1003—7985

Parametric analysis of the nonlinear primary resonance of spatial cable suspension bridges

Hui Yi[1] Xu Liang[2]

([1]School of Civil Engineering, Chongqing University, Chongqing 400030, China)
([2]School of Civil Engineering, Suzhou University of Science and Technology, Suzhou 215011, China)

Abstract: A comprehensive model based on continuum theory is adopted to conduct the parametric analysis of the primary resonance of the nonlinear vibration of spatial cable suspension bridges. This model can simultaneously account for the geometric nonlinearity of both the vertical motion of the deck and the vertical-horizontal motion of the cable. Based on this model and the multiple scale method (MSM), the modulation equations of the primary resonance responses are derived for spatial cable suspension bridges. Nonlinear coefficients in the modulation equations are determined to have notable influences on the maximum response amplitude of the primary resonance of the system and the hardening or softening characteristics of the investigated vibration mode. Meanwhile, system parameters, such as the inclination angles of the main cable and hanger, the sag-to-span ratio of the cable, and the tensile stiffness ratio between the deck and cable, can notably influence the nonlinear coefficient. The dynamic properties of the system can change dramatically in the form of sudden changes in the nonlinear coefficient of the symmetric vibration of the deck and cable if the parameter is located near the singularity, which should be avoided in the design of the system. This study can provide reference for the design of the bridge structure.

Key words: suspension bridge; spatial cable; nonlinear dynamics; multiple scale method; primary resonance
DOI: 10.3969/j.issn.1003 - 7985.2024.02.007

A suspension bridge is a system sensitive to dynamic loads because of its light weight and flexibility, in which nonlinear vibration is inevitable under common loads, such as crowd and automobile forces[1-4]. Many studies of the nonlinear dynamics of suspension bridges based on mathematical models have been conducted in the past few decades. Contributions to this research include but are not limited to those of Abdel-Ghaffar and Rubin[5-6] and Çevik and Pakdemirli[7], who analyzed the nonlinear free and forced, coupled vertical-torsional vibrations of suspension bridges utilizing the multiple scale method. Lazer and McKenna[8] analyzed the nonlinear, large-amplitude periodic oscillations detected within such structures. Further contributions to this research came from Capsoni et al.[9-10], who investigated the torsionally aeroelastic and parametric resonance instabilities of suspension bridges using the multiple scale method based on the nonlinear continuum model, specifically considering vertically planar configurations. Lepidi and Gattulli[11] analyzed the nonlinear interactions between the main cables and the deck of a suspension bridge. In addition, Peng et al.[12] thoroughly inspected the nonlinear primary resonance of a cable-supported beam, particularly under time delay feedback conditions.

Studies of nonlinear dynamics were mainly focused on conventional suspension bridges with vertical cable configurations. However, recent advancements have led to the construction of bridges with spatial geometric layouts of the main cables[13]. These bridges exhibit dynamic behavior that differs from that of conventional models, with cables supporting the deck in both vertical and lateral directions. Such configurations compel additional scrutiny into the relative motion between cable and deck because of the spatialization of cables. Notably, inclined cables and hangers may enhance the nonlinear vibration of the structure. In their work, Hui et al.[14-15] conceived a six-degrees-of-freedom (DoF) sectional model and a seven-DoF model to examine the primary and internal resonances of suspension bridges using the incremental harmonic balance method.

To capture the dynamic behavior of the bridge in a spanwise manner, Xu et al.[16] proposed a mathematical model of a full bridge for a spatially supported bridge deck. This model aids in establishing the geometric configuration in a static balance state and facilitating modal analysis. However, the complexity of this model may limit its applicability to nonlinear dynamic analysis because of its detailed considerations of bridge component modeling. Nevertheless, these researchers proposed a simplified model to examine the primary and nonlinear resonance scenarios of vertical vibration, with two main

Received 2023-11-03, **Revised** 2024-03-15.

Biography: Hui Yi (1985—), male, doctor, professor, alihui@cqu.edu.cn.

Foundation items: The Scientific Research Foundation of Suzhou University of Science and Technology (No. 332311106), the National Natural Science Foundation of China (No. 52078087), 111 Project of the Ministry of Education and the Bureau of Foreign Experts of China (No. B18062).

Citation: Hui Yi, Xu Liang. Parametric analysis of the nonlinear primary resonance of spatial cable suspension bridges[J]. Journal of Southeast University (English Edition), 2024, 40(2): 165 - 175. DOI: 10.3969/j.issn.1003 - 7985.2024.02.007.

cables harmoniously vibrating in both vertical and horizontal directions, as reported in Refs. [17 − 18]. This model was subsequently refined to address the primary resonance of torsional vibration along with coupled vertical-torsional vibrations of suspension bridges[19].

Because the subjects, i.e., humans or vehicles, acting on the bridge are most sensitive to the vertical vibration of the deck[20], this study adopts the model proposed by Xu et al.[17] to provide sufficient nonlinear dynamic information on spatial cable suspension bridges. For a nonlinear system, the multiple scale method is always adopted to calculate the dynamic responses, as it can provide a more comprehensive understanding of the dynamic features of the system. In this case, the nonlinear coefficient is a crucial factor for the analysis. However, the impact of the nonlinear coefficient on such a bridge system remains poorly understood, and how the system parameters affect the nonlinear coefficient is still unclear, which significantly hinders insights into their nonlinear dynamic behavior. Therefore, this study intended to address this issue based on the earlier model.

This paper is organized as follows: First, the formula of the continuum model is revisited. Based on this model and the multiple scale method, the modulation equations accounting for the primary resonance responses of such a system are derived. Then, the influence of nonlinear coefficients in the modulation equations on the maximum response amplitude of the primary resonance of three typical modes under external vertical loads is examined. Parametric analysis of the influence of the system parameters, such as the inclination angles of the cables, the sag-to-span ratio of the cable, and the tensile stiffness ratio between deck and cable, on the nonlinear coefficients is conducted. Finally, some key conclusions are given at the end of this study.

1 Mathematical Model

The spatial cable suspension bridge shown in Fig. 1(a) is taken as the research object of this study. Xu et al.[17] proposed its model as depicted in Fig. 1(b). In alignment with engineering practices, this study considers only shallow cables, where the sag-to-span ratio of the main cable is less than 1/8 ($d/l < 1/8$, where d is the initial sag of the main cable and l is the length of the main span of the bridge). In this model, the hangers are replaced by a massless continual membrane, which is assumed to be rigid without any deformation. Both cables and deck were assumed to be simply supported at two ends. A cartesian coordinate system, denoted by $\boldsymbol{e}_i$ (where $i = 1, 2, 3$), is used to define the position of the structure. The coordinates of the cables and deck in the statically balanced configuration (labeled as T^{I}) can be expressed as $\boldsymbol{X}_{\mathrm{c}}^{\mathrm{I}}(s_{\mathrm{c}}^{\mathrm{I}}) = y_{e1}\boldsymbol{e}_1 + y_{e2}\boldsymbol{e}_2 + x\boldsymbol{e}_3$ and $\boldsymbol{X}_{\mathrm{d}}^{\mathrm{I}}(s_{\mathrm{d}}^{\mathrm{I}}) = 0\boldsymbol{e}_1 + 0\boldsymbol{e}_2 + x\boldsymbol{e}_3$, where the subscripts c and d denote the main cables and deck, respectively. y_{e1} and y_{e2} are the projections of the spatial cable on the horizontal ($\boldsymbol{e}_1$-0-$\boldsymbol{e}_3$) and vertical ($\boldsymbol{e}_2$-0-$\boldsymbol{e}_3$) planes, respectively, and x is the coordinate along $\boldsymbol{e}_3$ of the bridge with a span l.

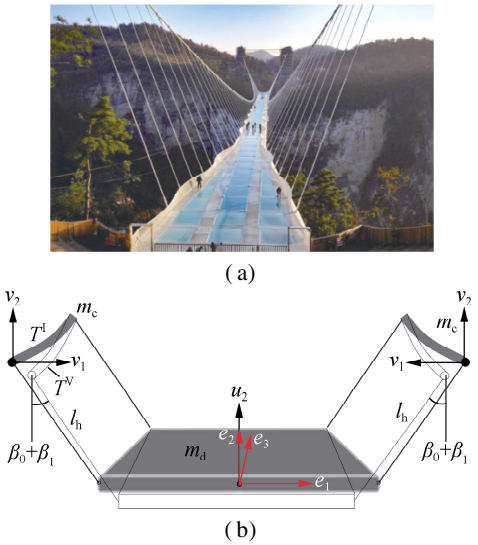

Fig. 1 Model of a suspension bridge with a spatial geometric layout of the main cables. (a) Zhangjiajie glass bridge; (b) Geometric schematic of the bridge model

The mathematical model of this type of bridge is briefly introduced in this section. The mass per unit length of the cables and deck are denoted as m_{c} and m_{d}, respectively. Using the shape-finding technique[16], the initial single cable tension projected in the horizontal direction, H, can be determined under the following conditions: Taking the assumption that the initial internal force in the bridge deck exists in a state of static equilibrium. Focusing on the symmetric movement of the cables and the vertical motion of the deck, we include the vertical and horizontal displacements of the main cable (labeled as v_1 and v_2, respectively) and the vertical displacement of the deck (u_2) in the motion description of the entire bridge structure (labeled as T^{V}). The corresponding damping factors are labeled as κ_{c} and κ_{d}. An external force (F_{d}) is hypothetically applied vertically on the deck.

By substituting the kinetic energy, potential energy, and work done by external forces into the extended Hamilton principle, the variation equations of the suspension bridge[17] can be expressed as follows:

$$-\int_{t_1}^{t_2}\int_0^l \{[2m_{\mathrm{c}}\ddot{v}_1 + 2\kappa_{\mathrm{c}}\dot{v}_1 - 2Hv_1'' - 2E_{\mathrm{c}}A_{\mathrm{c}}e_{\mathrm{c}}(t)(y_{e1}'' + v_1'')]\delta v_1 + \{2m_{\mathrm{c}}\ddot{v}_2 + 2\kappa_{\mathrm{c}}\dot{v}_2 - 2Hv_2'' - 2E_{\mathrm{c}}A_{\mathrm{c}}e_{\mathrm{c}}(t)(y_{e2}'' + v_2'')\}\delta v_2 + [m_{\mathrm{d}}\ddot{u}_2 + \kappa_{\mathrm{d}}\dot{u}_2 - E_{\mathrm{d}}A_{\mathrm{d}}u_2''e_{\mathrm{d}}(t) + E_{\mathrm{d}}J_{e1}u_2^{(4)} - F_{\mathrm{d}}]\delta u_2\}\mathrm{d}x\mathrm{d}t = 0 \quad (1)$$

where E_c and E_d are the elastic moduli of the materials for the cables and deck, respectively; A_c and A_d are the cross-sections of the cables and deck, respectively; J_{e1} is the moment of inertia of the deck section about axis $\boldsymbol{e}_1$; F_d is the time-dependent external force. The overdot and prime indicate the derivatives of time t and x, respectively. $e_c(t)$ and $e_d(t)$ expressed in Eq. (1) are rewritten as follows:

$$e_c(t) = \frac{1}{l}\int_0^l \left\{ y'_{e1}v'_1 + y'_{e2}v'_2 + \frac{1}{2}[(v'_1)^2 + (v'_2)^2] \right\} \mathrm{d}x \tag{2a}$$

$$e_d(t) = \frac{1}{l}\int_0^l \frac{1}{2}(u'_2)^2 \mathrm{d}x \tag{2b}$$

Given that the hangers are assumed to be rigid, v_1 and u_2 can be expressed as functions of v_2, β_0, and β_1 as follows:

$$v_1 = l_h \sin\beta_0 - l_h \sin(\beta_0 + \beta_1) \tag{3a}$$

$$u_2 = v_2 - l_h \cos(\beta_0 + \beta_1) + l_h \cos\beta_0 \tag{3b}$$

where β_0 is the inclination angle of hangers in the vertical direction in the static balanced state; β_1 is the increment of the inclination of the hanger due to vibration in the dynamic state; and $l_h(x)$ is the length of the hanger in position x.

When considering the small dynamic angular displacement β_1 of the hanger, the following equations can be derived:

$$\sin(\beta_0 + \beta_1) \approx \sin\beta_0 + \beta_1 \cos\beta_0 \tag{4a}$$

$$\cos(\beta_0 + \beta_1) \approx \cos\beta_0 - \beta_1 \sin\beta_0 \tag{4b}$$

Based on Eq. (4), Eq. (3) can be rewritten as follows:

$$u_2 = bv_1 + v_2 \tag{5a}$$

$$\delta u_2 = b\delta v_1 + \delta v_2 \tag{5b}$$

where $b = \tan\beta_0$.

Eq. (5) is substituted into Eq. (1), and $F_d = f_d \cos(\Omega t)$, in which f_d and Ω are the amplitude and excitation frequency, respectively, is considered. Based on some basic manipulation of integration by parts and variational operations, the following equations can be obtained by solving the nontrivial solutions of the Lagrange variational equations:

$$\begin{aligned}&(2m_c + m_d b^2)\ddot{v}_1 + m_d b\,\ddot{v}_2 + (2\kappa_c + \kappa_d b^2)\dot{v}_1 + \kappa_d b\,\dot{v}_2 - 2Hv''_1 - 2E_cA_c(y_{e1} + v_1)''e_c(t) - \\ &E_dA_d b(bv_1 + v_2)''e_d(t) + E_dJ_{e1}b(bv_1 + v_2)^{(4)} - bf_d\cos(\Omega t) = 0\end{aligned} \tag{6a}$$

$$\begin{aligned}&(2m_c + m_d)\ddot{v}_2 + m_d b\,\ddot{v}_1 + (2\kappa_c + \kappa_d)\dot{v}_2 + \kappa_d b\,\dot{v}_1 - 2Hv''_2 - 2E_cA_c(y_{e2} + v_2)''e_c(t) - \\ &E_dA_d(bv_1 + v_2)''e_d(t) + E_dJ_{e1}(bv_1 + v_2)^{(4)} - f_d\cos(\Omega t) = 0\end{aligned} \tag{6b}$$

The following nondimensional quantities are introduced for the nonlinear dynamic analysis:

$$\begin{aligned}&\bar{x} = \frac{x}{l},\ \Omega_0 = \frac{1}{l\sqrt{H/m_c}},\ \bar{t} = \Omega_0 t,\ \bar{y}_{e1} = \frac{y_{e1}}{l},\ \bar{y}_{e2} = \frac{y_{e2}}{l},\ \bar{u}_2 = \frac{b_1v_1 + b_2v_1^2 + b_3v_1^3 + v_2}{l} \\ &\bar{v}_1 = \frac{v_1}{l},\ \bar{v}_2 = \frac{v_2}{l},\ \alpha_c = \frac{E_cA_c}{H},\ \alpha_d = \frac{E_dA_d}{H},\ \tau_d = \frac{E_dJ_{e1}}{Hl^2},\ r_m = \frac{m_d}{m_c} \\ &\eta_c = \kappa_c\sqrt{\frac{l^2}{m_cH}},\ \eta_d = \kappa_d\sqrt{\frac{l^2}{m_cH}},\ \bar{b}_1 = \tan\beta_0,\ \bar{f}_d = \frac{f_dl}{H},\ \bar{\Omega} = \frac{\Omega}{\Omega_0}\end{aligned} \tag{7}$$

The overbars of the variables in Eq. (7) are disregarded hereafter for the sake of convenience. The substitution of Eq. (7) into Eq. (6) yields the following set of equations of motion:

$$\begin{aligned}&(2 + r_m b^2)\ddot{v}_1 + r_m b\,\ddot{v}_2 + (2\eta_c + \eta_d b^2)\dot{v}_1 + \eta_d b\,\dot{v}_2 - 2v''_1 - 2\alpha_c(y_{e1} + v_1)''e_c(t) - \\ &\alpha_d b(bv_1 + v_2)''e_d(t) + \tau b(bv_1 + v_2)^{(4)} - bf_d\cos(\Omega t) = 0\end{aligned} \tag{8a}$$

$$\begin{aligned}&(2 + r_m)\ddot{v}_2 + r_m b\,\ddot{v}_1 + (2\eta_c + \eta_d)\dot{v}_2 + \eta_d b\,\dot{v}_1 - 2v''_2 - 2\alpha_c(y_{e2} + v_2)''e_c(t) - \\ &\alpha_d(bv_1 + v_2)''e_d(t) + \tau_d(bv_1 + v_2)^{(4)} - f_d\cos(\Omega t) = 0\end{aligned} \tag{8b}$$

$$e_c(t) = \int_0^1 \left\{ y'_{e1}v'_1 + y'_{e2}v'_2 + \frac{1}{2}[(v'_1)^2 + (v'_2)^2] \right\} \mathrm{d}x \tag{9a}$$

$$e_d(t) = \int_0^1 \frac{1}{2}\left[(bv_1 + v_2)' \right]^2 \mathrm{d}x \tag{9b}$$

The boundary conditions for the hinge-supported cables and deck can be written as follows:

$$v_i(0,t) = v_i(1,t) = v''_i(0,t) = v''_i(1,t) = 0 \qquad i = 1,2 \tag{10}$$

For the details of the derivation of the bridge model, the readers can refer to Ref. [17].

2 Theory of Response Perturbation

Notably, the dynamic equations of the continuous sys-

tem (Eq. (8)) exhibit a coupled nonlinear relationship, denoted as v_1 and v_2. To reveal the nonlinear dynamics of this system, the multiple scale method[21-22] is employed to solve these dynamic equations. This analytical technique is crucial for addressing nonlinear problems in mathematical models, especially in nonlinear vibration analysis, because it decomposes the dynamics of a system into distinct temporal scales, enabling a more nuanced and comprehensive understanding of its behavior. In this analysis, the multiple scale method is applied, and its solutions are expressed in the following forms:

$$v_1 = \sum_{i=1}^{3} \varepsilon^i g_i(x, T_0, T_1, T_2) \tag{11a}$$

$$v_2 = \sum_{i=1}^{3} \varepsilon^i q_i(x, T_0, T_1, T_2) \tag{11b}$$

$$T_j = \varepsilon^j t \qquad j = 0, 1, 2 \tag{11c}$$

where ε is a small positive value, and the superscript of ε denotes its power. g_i and $q_i (i = 1, 2, 3)$ are the displacement components in the i-th-order time scale. The damping and forcing terms in Eq. (8) are scaled such that their influences balance the influence of nonlinearities. Hence, the dimensionless damping coefficients of cable and deck (η_c, η_d) and the external force (f_d) are rescaled as $\eta_c \to \varepsilon^2 \eta_c$, $\eta_d \to \varepsilon^2 \eta_d$, and $f_d \to \varepsilon^2 f_d$, respectively. The derivatives of time are written as follows:

$$\frac{\mathrm{d}}{\mathrm{d}t} = D_0 + \varepsilon D_1 + \varepsilon^2 D_2 + \dots$$

$$\frac{\mathrm{d}^2}{\mathrm{d}t^2} = D_0^2 + 2\varepsilon D_0 D_1 + \varepsilon^2 (D_1^2 + 2D_0 D_2) + \dots \tag{12}$$

where $D_j = \dfrac{\partial}{\partial T_j} (j = 0, 1, 2)$.

Eqs. (11) and (12) are substituted into Eq. (8), and terms with different ε^j are grouped and rearranged. The following differential equations can be obtained, considering coefficients of ε^1, ε^2, and ε^3 being zero.

Coefficient of the first-order term ε^1 is

$$l_1(g_1, q_1) = (2 + r_m b^2) D_0^2 g_1 + r_m b D_0^2 q_1 - 2g_1'' - 2\alpha_c y_{e1}'' \int_0^1 (y_{e1}' g_1' + y_{e2}' q_1') \,\mathrm{d}x + \tau_d b (b g_1 + q_1)^{(4)} = 0 \tag{13a}$$

$$l_2(g_1, q_1) = (2 + r_m) D_0^2 q_1 + r_m b D_0^2 g_1 - 2q_1'' - 2\alpha_c y_{e2}'' \int_0^1 (y_{e1}' g_1' + y_{e2}' q_1') \,\mathrm{d}x + \tau_d (b g_1 + q_1)^{(4)} = 0 \tag{13b}$$

Coefficient of the second-order term ε^2 is

$$l_1(g_2, q_2) = 2\alpha_c g_1'' \int_0^1 (y_{e1}' g_1' + y_{e2}' q_1') \,\mathrm{d}x + \alpha_c y_{e1}'' \int_0^1 [(g_1')^2 + (q_1')^2] \,\mathrm{d}x \tag{14a}$$

$$l_2(g_2, q_2) = 2\alpha_c q_1'' \int_0^1 (y_{e1}' g_1' + y_{e2}' q_1') \,\mathrm{d}x + \alpha_c y_{e2}'' \int_0^1 [(g_1')^2 + (q_1')^2] \,\mathrm{d}x \tag{14b}$$

Coefficient of the third-order term ε^3 is

$$\begin{aligned} l_1(g_3, q_3) = {} & -D_0[(2\eta_c + \eta_d b^2) g_1 + \eta_d b q_1] - 2D_0 D_2[(2 + r_m b^2) g_1 + r_m b q_1] + \\ & \frac{\alpha_d}{2} b (b g_1 + q_1)'' \int_0^1 [(b g_1 + q_1)']^2 \mathrm{d}x + 2\alpha_c y_{e1}'' \int_0^1 (g_1' g_2' + q_1' q_2') \,\mathrm{d}x + \alpha_c g_1'' \int_0^1 [(g_1')^2 + (q_1')^2] \,\mathrm{d}x + \\ & 2\alpha_c g_2'' \int_0^1 (y_{e1}' g_1' + y_{e2}' q_1') \,\mathrm{d}x + 2\alpha_c g_1'' \int_0^1 (y_{e1}' g_2' + y_{e2}' q_2') \,\mathrm{d}x + b f_d \cos(\Omega T_0) \end{aligned} \tag{15a}$$

$$\begin{aligned} l_2(g_3, q_3) = {} & -D_0[\eta_d b g_1 + (2\eta_c + \eta_d) q_1] - 2D_0 D_2[r_m b g_1 + (2 + r_m) q_1] + \\ & \frac{\alpha_d}{2} (b g_1 + q_1)'' \int_0^1 (b g_1 + q_1)'^2 \mathrm{d}x + 2\alpha_c y_{e2}'' \int_0^1 (g_1' g_2' + q_1' q_2') \,\mathrm{d}x + \alpha_c q_1'' \int_0^1 [(g_1')^2 + (q_1')^2] \,\mathrm{d}x + \\ & 2\alpha_c q_2'' \int_0^1 (y_{e1}' g_1' + y_{e2}' q_1') \,\mathrm{d}x + 2\alpha_c q_1'' \int_0^1 (y_{e1}' g_2' + y_{e2}' q_2') \,\mathrm{d}x + f_d \cos(\Omega T_0) \end{aligned} \tag{15b}$$

with the following boundary conditions:

$$g_i \big|_{x=0,1} = 0, \; q_i \big|_{x=0,1} = 0 \qquad i = 1, 2, 3 \tag{16}$$

The general solutions of Eqs. (13a) and (13b) can be expressed as follows:

$$g_1(x, T_0, T_2) = A(T_2) \varphi_{v1}(x) \mathrm{e}^{\mathrm{i}\omega_0 T_0} + \phi_{cc} \tag{17a}$$

$$q_1(x, T_0, T_2) = A(T_2) \varphi_{v2}(x) \mathrm{e}^{\mathrm{i}\omega_0 T_0} + \phi_{cc} \tag{17b}$$

where ϕ_{cc} is the complex conjugate of the preceding term on the right-hand side of the equation, and φ_{v1} and φ_{v2} are the mode shapes of cable in the vertical and horizontal directions, respectively. ω_0 is the selected eigenfrequency. $A(T_2)$ is the complex modal amplitude, which will be written as A hereafter for convenience. By substituting Eq. (17) into Eq. (14), we derive the following expressions:

$$l_1(g_2, q_2) = \left\{2\alpha_c\varphi''_{v1}\int_0^1 (y'_{e1}\varphi'_{v1} + y'_{e2}\varphi'_{v2})\,dx + \alpha_c y''_{e1}\int_0^1 [(\varphi'_{v1})^2 + (\varphi'_{v2})^2]\,dx\right\}(A^2 e^{2i\omega_0 T_0} + A\bar{A} + \phi_{cc}) \quad (18a)$$

$$l_2(g_2, q_2) = \left\{2\alpha_c\varphi''_{v2}\int_0^1 (y'_{e1}\varphi'_{v1} + y'_{e2}\varphi'_{v2})\,dx + \alpha_c y''_{e2}\int_0^1 [(\varphi'_{v1})^2 + (\varphi'_{v2})^2]\,dx\right\}(A^2 e^{2i\omega_0 T_0} + A\bar{A} + \phi_{cc}) \quad (18b)$$

Similarly, the solutions of Eqs. (14a) and (14b) can be expressed in the following forms:

$$g_2(x, T_0, T_2) = \psi_{11}(A^2 e^{2iT_0\omega_m} + cc) + \psi_{12}A\bar{A} \quad (19a)$$

$$q_2(x, T_0, T_2) = \psi_{21}(A^2 e^{2iT_0\omega_0} + cc) + \psi_{22}A\bar{A} \quad (19b)$$

where $\psi_{ij}(i, j = 1, 2)$ is the second-order shape function. The following expressions can be obtained when the solutions of Eqs. (14a) and (14b) are substituted separately into Eq. (19):

$$-4\omega_0^2(2 + r_m b^2)\psi_{11} - 4\omega_0^2 r_m b\psi_{21} - 2\psi''_{11} - 2\alpha_c y''_{e1}\int_0^1 (y'_{e1}\psi'_{11} + y'_{e2}\psi'_{21})\,dx + \tau_d b[(b\psi_{11})^{(4)} + \psi_{21}^{(4)}] = \Pi_1 \quad (20a)$$

$$-4\omega_0^2(2 + r_m)\psi_{21} - 4\omega_0^2 r_m b\psi_{11} - 2\psi''_{21} - 2\alpha_c y''_{e2}\int_0^1 (y'_{e1}\psi'_{11} + y'_{e2}\psi'_{21})\,dx + \tau_d[(b\psi_{11})^{(4)} + \psi_{21}^{(4)}] = \Pi_2 \quad (20b)$$

$$-2\psi''_{21} - 2\alpha_c y''_{e1}\int_0^1 (y'_{e1}\psi'_{12} + y'_{e2}\psi'_{22})\,dx + \tau_d b[(b\psi_{21})^{(4)} + \psi_{22}^{(4)}] = 2\Pi_1 \quad (21a)$$

$$-2\psi''_{22} - 2\alpha_c y''_{e2}\int_0^1 (y'_{e1}\psi'_{12} + y'_{e2}\psi'_{22})\,dx + \tau_d[(b\psi_{21})^{(4)} + \psi_{22}^{(4)}] = 2\Pi_2 \quad (21b)$$

where

$$\Pi_1 = 2\alpha_c\varphi''_{v1}\int_0^1 (y'_{e1}\varphi'_{v1} + y'_{e2}\varphi'_{v2})\,dx + \alpha_c y''_{e1}\int_0^1 [(\varphi'_{v1})^2 + (\varphi'_{v2})^2]\,dx \quad (22a)$$

$$\Pi_2 = 2\alpha_c\varphi''_{v2}\int_0^1 (y'_{e1}\varphi'_{v1} + y'_{e2}\varphi'_{v2})\,dx + \alpha_c y''_{e2}\int_0^1 [(\varphi'_{v1})^2 + (\varphi'_{v2})^2]\,dx \quad (22b)$$

Primary resonance occurs when the excitation frequency Ω is close to the target modal frequency ω_0. A detuning parameter σ can be introduced[23] such that

$$\Omega = \omega_0 + \varepsilon^2\sigma \quad (23)$$

where ε^2 has a small value, the same as that defined in Eq. (23).

By substituting Eqs. (17) and (19) into Eq. (15), we derive the following expressions:

$$l_1(g_3, q_3) = h_1(x, T_2)e^{i\omega_0 T_0} + cc + \phi_{NST} \quad (24a)$$

$$l_2(g_3, q_3) = h_2(x, T_2)e^{i\omega_0 T_0} + cc + \phi_{NST} \quad (24b)$$

where ϕ_{NST} are terms that do not produce secular terms. The terms $h_1(x, T_2)$ and $h_2(x, T_2)$ can be rewritten as follows:

$$\begin{aligned} h_1(x, T_2) = {} & -i\omega_0\{[(2\eta_c + \eta_d b^2)\varphi_{v1} + \eta_d b\varphi_{v2}]A + [2(2 + r_m b^2)\varphi_{v1} + 2r_m b\varphi_{v2}]\dot{A}\} + \\ & \frac{3\alpha_d}{2}b(b\varphi_{v1} + \varphi_{v2})''\int_0^1 [(b\varphi_{v1} + \varphi_{v2})']^2 dx A^2\bar{A} + \\ & 2\alpha_c y''_{e1}\int_0^1 (\varphi'_{v1}\psi'_{11} + \varphi'_{v2}\psi'_{21})\,dx\bar{A}A^2 + 4\alpha_c y''_{e1}\int_0^1 (\varphi'_{v1}\psi'_{12} + \varphi'_{v2}\psi'_{22})\,dxAA\bar{A} + \\ & 3\alpha_c\varphi''_{v1}\int_0^1 [(\varphi'_{v1})^2 + (\varphi'_{v2})^2]\,dx A^2\bar{A} + 2\alpha_c\psi''_{11}\int_0^1 (y'_{e1}\varphi'_{v1} + y'_{e2}\varphi'_{v2})\,dx A^2\bar{A} + \\ & 2\alpha_c\psi''_{12}\int_0^1 (y'_{e1}\varphi'_{v1} + y'_{e2}\varphi'_{v2})\,dxA\bar{A}A + 4\alpha_c\varphi''_{v1}\int_0^1 (y'_{e1}\psi'_{22} + y'_{e2}\psi'_{12})\,dxAA\bar{A} + \\ & 2\alpha_c\varphi''_{v1}\int_0^1 (y'_{e1}\psi'_{21} + y'_{e2}\psi'_{11})\,dx\bar{A}A^2 + \frac{1}{2}bf_d e^{i\sigma T_2} \end{aligned} \quad (25a)$$

$$\begin{aligned} h_2(x, T_2) = {} & -i\omega_0\{[(2\eta_c + \eta_d)\varphi_{v2} + \eta_d b\varphi_{v1}]A + [2(2 + r_m)\varphi_{v2} + 2r_m b\varphi_{v1}]\dot{A}\} + \\ & \frac{3\alpha_d}{2}(b\varphi_{v1} + \varphi_{v2})''\int_0^1 [(b\varphi_{v1} + \varphi_{v2})']^2 dx A^2\bar{A} + \\ & 2\alpha_c y''_{e2}\int_0^1 (\varphi'_{v1}\psi'_{11} + \varphi'_{v2}\psi'_{21})\,dx\bar{A}A^2 + 4\alpha_c y''_{e2}\int_0^1 (\varphi'_{v1}\psi'_{12} + \varphi'_{v2}\psi'_{22})\,dxAA\bar{A} + \\ & 3\alpha_c\varphi''_{v2}\int_0^1 [(\varphi'_{v1})^2 + (\varphi'_{v2})^2]\,dx A^2\bar{A} + 2\alpha_c\psi''_{21}\int_0^1 (y'_{e1}\varphi'_{v1} + y'_{e2}\varphi'_{v2})\,dx A^2\bar{A} + \end{aligned}$$

$$2\alpha_c\psi''_{22}\int_0^1 (y'_{e1}\varphi'_{v1} + y'_{e2}\varphi'_{v2})\,\mathrm{d}x A\bar{A}A + 4\alpha_c\varphi''_{v2}\int_0^1 (y'_{e1}\psi'_{12} + y'_{e2}\psi'_{22})\,\mathrm{d}x AA\bar{A} +$$
$$2\alpha_c\varphi''_{v2}\int_0^1 (y'_{e1}\psi'_{21} + y'_{e2}\psi'_{11})\,\mathrm{d}x\bar{A}A^2 + \frac{1}{2}f_d e^{i\sigma T_2} \tag{25b}$$

Eq. (24) is a nonhomogeneous equation, and its nontrivial solutions become φ_{v1} and φ_{v2} based on Eq. (13) when the solvability condition can be satisfied as follows according to Ref. [23]:

$$\int_0^1 [\varphi_{v1}h_1(x, T_2) + \varphi_{v2}h_2(x, T_2)]\,\mathrm{d}x \equiv 0 \tag{26}$$

Therefore, by substituting $h_1(x, T_2)$ and $h_2(x, T_2)$ into Eq. (26), we derive the following expression:

$$2i\omega_0\Gamma_1\dot{A} + 2i\omega_0\Gamma_2 A + \Gamma_3 A^2\bar{A} = \frac{1}{2}f_r e^{i\sigma T_2} \tag{27}$$

where $\Gamma_i (i = 1, 2, 3)$ are nonlinear coefficients derived as follows:

$$\Gamma_1 = \int_0^1 [(2 + r_m b^2)\varphi_{v1}^2 + 2r_m b\varphi_{v1}\varphi_{v2} + (2 + r_m)\varphi_{v2}^2]\,\mathrm{d}x \tag{28a}$$

$$\Gamma_2 = \int_0^1 \left[\left(\eta_c + \frac{\eta_d b^2}{2}\right)\varphi_{v1}^2 + \eta_d b\varphi_{v1}\varphi_{v2} + \left(\eta_c + \frac{\eta_d}{2}\right)\varphi_{v2}^2\right]\mathrm{d}x \tag{28b}$$

$$\Gamma_3 = \Gamma_{31} + \Gamma_{32} \tag{28c}$$

where

$$\Gamma_{31} = \frac{3\alpha_d}{2}\left\{\int_0^1 [(b\varphi_{v1} + \varphi_{v2})']^2\mathrm{d}x\right\}^2 \tag{29a}$$

$$\begin{aligned}\Gamma_{32} = {} & 3\alpha_c\left\{\int_0^1 [(\varphi'_{v1})^2 + (\varphi'_{v2})^2]\,\mathrm{d}x\right\}^2 + 2\alpha_c\int_0^1 (\varphi'_{v1}\psi'_{11} + \varphi'_{v2}\psi'_{21})\,\mathrm{d}x\int_0^1 (y'_{e1}\varphi'_{v1} + y'_{e2}\varphi'_{v2})\,\mathrm{d}x + \\ & 2\alpha_c\int_0^1 (y'_{e1}\varphi'_{v1} + y'_{e2}\varphi'_{v2})\,\mathrm{d}x\left(\int_0^1 (\varphi'_{v1}\psi'_{11} + \varphi'_{v2}\psi'_{21})\,\mathrm{d}x + \int_0^1 (\varphi'_{v1}\psi'_{12} + \varphi'_{v2}\psi'_{22})\,\mathrm{d}x\right) + \\ & 2\alpha_c\int_0^1 [(\varphi'_{v1})^2 + (\varphi'_{v2})^2]\,\mathrm{d}x\left[\int_0^1 (y'_{e1}\psi'_{11} + y'_{e2}\psi'_{21})\,\mathrm{d}x + \int_0^1 (y'_{e1}\psi'_{12} + y'_{e2}\psi'_{22})\,\mathrm{d}x\right] + \\ & 2\alpha_c\int_0^1 (\varphi'_{v1}\psi'_{12} + \varphi'_{v2}\psi'_{22})\,\mathrm{d}x\int_0^1 (y'_{e1}\varphi'_{v1} + y'_{e2}\varphi'_{v2})\,\mathrm{d}x\end{aligned} \tag{29b}$$

Notably, all of the investigated mode shapes can be normalized with Γ_1 equal to unity. Γ_{31} is a property of the bridge deck, and Γ_{32} is a property of the cables. Their summation is the coefficient Γ_3, which has a strong influence on the hardening or softening behavior of the system. They are factors representing the mass, damping, and nonlinear stiffness. The term $\Gamma_i (i = 1, 2, 3)$ is dependent on the system modes. Force f_r can be expressed as follows:

$$f_r = \int_0^1 f_d(b\varphi_{v1} + \varphi_{v2})\,\mathrm{d}x \tag{30}$$

where f_d is the modal force of the target mode, and $b\varphi_{v1} + \varphi_{v2}$ is the vertical component of the mode shape of the deck, which can be deduced based on Eq. (5a).

The complex modal amplitude A is assumed to have the following form:

$$A = \frac{1}{2}ae^{i\vartheta} \tag{31}$$

We substitute Eq. (31) into Eq. (27) and separate the terms into real and imaginary parts to obtain the following modulation equations:

$$\dot{a} = \frac{f_r}{2\omega_0\Gamma_1}\sin\gamma - \frac{\Gamma_2}{\Gamma_1}a \tag{32a}$$

$$\dot{a}\gamma = a\sigma + \frac{f_r}{2\omega_0\Gamma_1}\cos\gamma - \frac{\Gamma_3}{8\omega_0\Gamma_1}a^3 \tag{32b}$$

where the prime symbol denotes the derivative of time T_2 and γ is a function of T_2 expressed as follows:

$$\gamma = \sigma T_2 - \vartheta \tag{33}$$

The variable γ is the phase of the solution to Eq. (27), which can be obtained together with a by solving Eq. (32) using the pseudo-arclength method[24].

3 Numerical Results

The proposed model is analyzed using the parameters listed in Table 1[25]. The numerical values of the dimensionless parameters of the system are obtained as $r_m = 13.22$, $\alpha_c = 6.28 \times 10^2$, $\alpha_d = 7.54 \times 10^3$, $\tau_d = 5.60 \times 10^{-3}$ based on Eq. (7). The ratio of the tension stiffness of the deck to the main cable is obtained as $r_\alpha = \alpha_d/\alpha_c = 12$. The aforementioned parameters are fixed hereafter unless otherwise stated. The damping terms in Eq. (8) are defined as $\eta_c = \eta_d = 0.1$. For the configurations of y_{e1} and y_{e2} of the main cables and the three lowest mode

shapes (ϕ_{v1} and ϕ_{v2}), i. e., first antisymmetric vertical mode of deck (1st ASVD), first symmetric vertical mode of deck (1st SVD), and first symmetric horizontal mode of cable (1st SHC), with the corresponding frequencies, the readers can refer to Ref. [17], and these mode shapes are also illustrated in Fig. 2.

Table 1 Material and geometric parameters

l/m	d	$\beta_0\|_{x=0,1}$/rad	m_c/kg	m_d/kg	r_m
430	1/10	$\pi/6$	385	5 080	13.21
E_d/GPa	J_{e1}/m^4	H/MN	A_c/m^2	A_d/m^2	E_c/GPa
210	7.13×10^{-2}	16.7	0.05	0.6	210

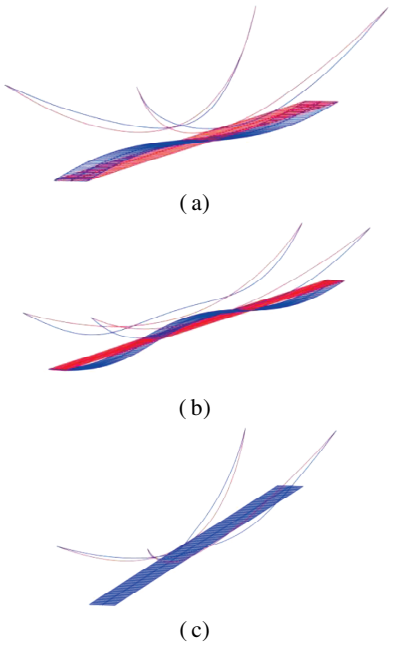

Fig. 2 Three typical mode shapes with $\beta_0\|_{x=0,l}=\pi/6$. (a) 1st ASVD($\omega=2.09$); (b) 1st SVD($\omega=3.33$); (c) 1st SHC($\omega=6.28$)

The second-order shape function $\psi_{ij}(i,\ j=1,2)$ corresponding to the primary resonance of the 1st ASVD mode, as shown in Fig. 3, can be calculated by numerically solving Eq. (32) using the nonlinear coefficients $\Gamma_1=1.0$, $\Gamma_2=0.021$, and $\Gamma_3=8.08\times10^4$.

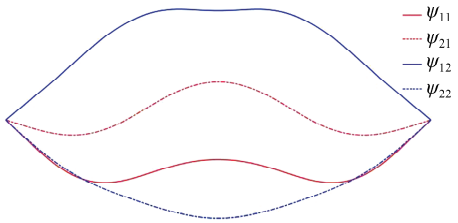

Fig. 3 Function $\psi_{ij}(i,j=1,2)$ for the primary resonance of the 1st ASVD mode

The three target modal responses of the bridge with $\beta_0\|_{x=0,l}=\pi/6$ are derived from Eq. (32) using both the MSM and Runge-Kutta methods combined with Galerkin discretization, as shown in Fig. 4. To ensure that the three modes have similar maximum response magnitude, f_r is equal to 5.0×10^{-4}, 1.2×10^{-3}, and 4.4×10^{-3} for the three cases selected. The results obtained by the two methods are noted to be consistent, except near the resonance, indicating the accurate application of the multiple scale method.

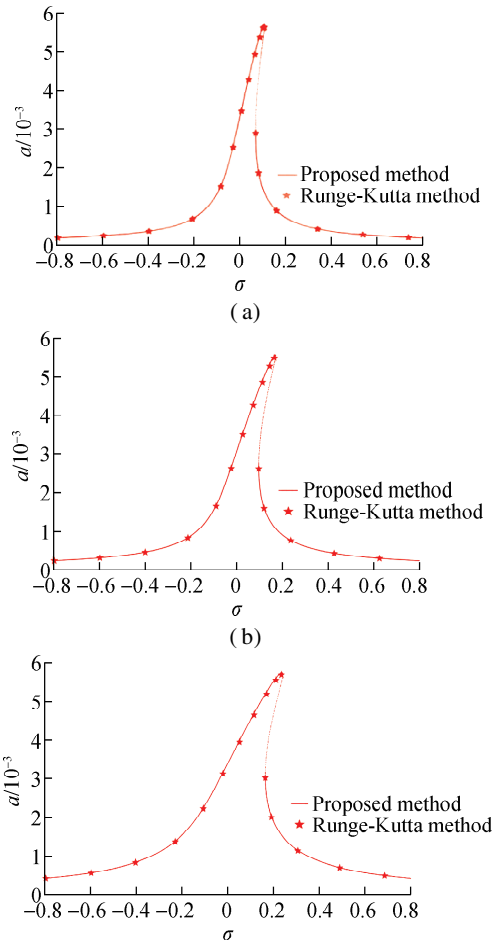

Fig. 4 Comparison of the amplitude-frequency curves of a suspension bridge with $\beta_0\|_{x=0,l}=\pi/6$ obtained using the proposed method and the Runge-Kutta method. (a) 1st ASVD, $f_r=5.0\times10^{-4}$ and $\omega_0=2.09$; (b) 1st SVD, $f_r=1.2\times10^{-3}$ and $\omega_0=3.33$; (c) 1st SHC, $f_r=4.4\times10^{-3}$ and $\omega_0=6.28$

The formulation in Eq. (28) shows that the nonlinear coefficient Γ_1 is always equal to unity, Γ_2 is a function of both damping coefficients (η_c and η_d) and mode shapes (ϕ_{v1} and ϕ_{v2}), and Γ_3 is a function of the mode shapes (ϕ_{v1} and ϕ_{v2}), the cable configurations (y_{e1} and y_{e2}), and the tensile stiffnesses of cables and deck (α_d and α_c).

The influences of these nonlinear coefficients on the resonance responses of a system are investigated in this section, with Γ_2 and Γ_3 having the values of (0.020 5, 0.041 0, 0.061 5, 0.082 0) and (-1.62×10^5, -8.08×10^4, 0, 8.08×10^4, 1.62×10^5), respectively. Their influences on the nonlinear dynamics of the 1st ASVD mode are illustrated in Figs. 5(a) and (b). The response amplitude is noted as dependent on Γ_2. The coefficient

Γ_2 is a complicated function, which is mainly related to system damping (because only the response peak in Fig. 5 (a) at resonance is affected, and there is no influence on the responses on the two sides). The coefficient Γ_3 is notably related to the nonlinear stiffness of the system with strong softening and hardening behavior at the primary resonance, confirming the observations of Çevik and Pakdemirli[7]. A positive Γ_3 is associated with "softening", and a negative Γ_3 is associated with "hardening". These phenomena increase with the absolute value of Γ_3.

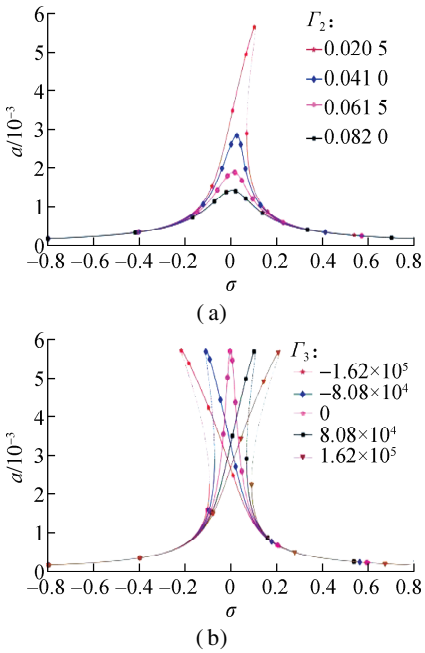

Fig. 5 Effects of Γ_2 and Γ_3 on the primary resonance response of the 1st ASVD mode with $\beta_0\big|_{x=0,\,l}=\pi/6$, $f_r=5.0\times10^{-4}$ and $\omega_0=2.09$. (a) Effect of Γ_2 with $\Gamma_3=8.08\times10^4$; (b) Effect of Γ_3 with $\Gamma_2=0.020\ 5$

Further examination of Eqs. (28) and (29) shows that Γ_3 consists of two terms, i.e., Γ_{31} and Γ_{32}. The first term is related to the dynamic properties of the deck, and the second term is associated with the dynamic properties of the main cables. Therefore, the influences of Γ_{31} and Γ_{32} corresponding to the 1st SHC mode are investigated with an example.

Notably, the sag-to-span ratio of cable (d) and the tensile stiffness ratio between deck and cable ($r_\alpha=\alpha_d/\alpha$) do not affect Γ_2. The effect of r_α on the terms Γ_{31} and Γ_{32} is analyzed and shown in Fig. 6. The practical range of $[1.0, 16.0]$ is selected for the ratio r_α. The coefficient Γ_{31} is noted to vary slowly with r_α, indicating a relatively stable influence from the bridge deck on the nonlinear features of the entire system. Conversely, Γ_{32} is noted to have a large variation with r_α at two particular values ($r_\alpha=3.9,\ 14.75$), which refers to a singularity that appears when the eigenfrequency of one system mode is twice that of the target mode. The curve of Γ_{32} varies asymptotically from $+\infty$ to $-\infty$ around these values of r_α. This phenomenon is consistent with the findings of the study conducted by Lacarbonara et al.[26] on the nonlinear vibration of a cable.

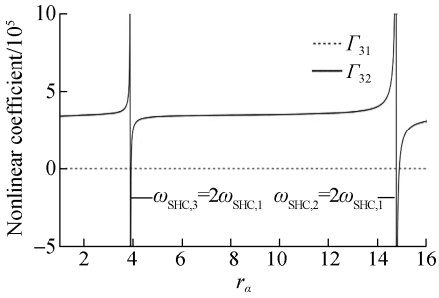

Fig. 6 Coefficients Γ_{31} and Γ_{32} for the 1st SHC mode as functions of the tensile stiffness ratio r_α when $\beta_0\big|_{x=0,\,l}=\pi/6$ and $d=1/10$

4 Effects of the System Parameters on the Nonlinear Coefficients

This section investigates the effects of the system parameters on the nonlinear coefficients Γ_2 and Γ_3. Three critical system parameters, namely the inclination angle of hangers (β_0), the sag-to-span ratio of cable (d), and the tensile stiffness ratio between deck and cable (r_α), are analyzed. The typical modes (i.e., 1st ASVD, 1st SVD, and 1st SHC) for the system discussed in Section 3 are examined. When there are changes in the system parameters, such as the inclination angle β_0 and the sag-to-span ratio d, the cable tension H, projections y_{e1} and y_{e2}, the dimensionless axial stiffnesses of deck α_c and cable α_d, and the flexural stiffness of deck τ_d should be recalculated according to the shape-finding technique and Eq. (7).

The value of β_0 before considering the self-weight of the main cable is taken to be in the range of 0-$\pi/4$ based on engineering practice with $r_\alpha=12$ and $d=1/10$. The other parameters are the same as those in Section 3. Fig. 7 shows that Γ_2 decreases by approximately 31% from 0.025 to 0.015 for the 1st ASVD mode when β_0 increases from 0 to $\pi/4$. Similarly, Γ_2 decreases by approximately 75% from 0.05 to 0.012 5 for the 1st SVD mode. However, Γ_2 increases from 0.01 to 0.038 for the 1st SHC mode. These results indicate that the effect of β_0 on Γ_2 is mode-dependent, which needs to be carefully examined in individual cases. Fig. 7 also shows the variations of Γ_{31} and Γ_{32} with β_0. Section 3 has concluded that the singularity in Γ_{32} dominates the behavior of the coefficient Γ_3, and this phenomenon is reexamined with the three modes investigated. Notably, singularity exists in all modes within the range of $\beta_0\in[0,\ \pi/4]$, except in the curve for the 1st ASVD mode. This finding indicates that the dynamic properties of the

system can change dramatically in the form of sudden changes in the symmetric vibration of the deck and cable if the parameter β_0 is located near the singularity, and this should be avoided in the design of the system.

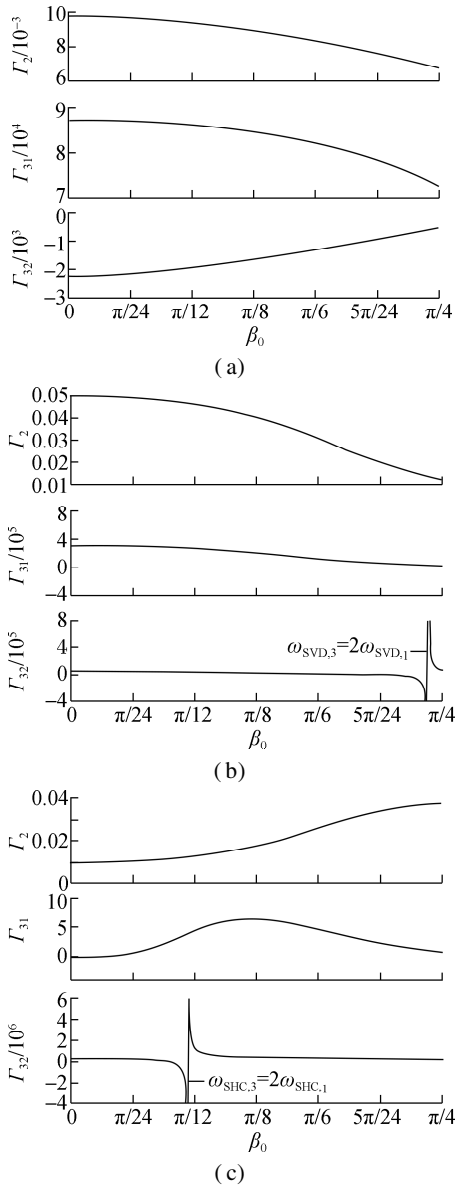

Fig. 7 Effect of β_0 on Γ_2, Γ_{31}, and Γ_{32} for different modes when $r_\alpha = 12$ and $d = 1/10$. (a) 1st ASVD; (b) 1st SVD; (c) 1st SHC

A similar study of the influence of parameter d on coefficient Γ_3 is conducted. Parameter d is selected with the practical range of 1/8 to 1/11. A range of inclination angle $\beta_0 \mid_{x=0,l} = (0,\ \pi/24,\ \pi/12,\ \pi/8,\ \pi/6,\ 5\pi/24,\ \pi/4)$ is selected with $r_\alpha = 12$. The other parameters are the same as those in Section 3. Fig. 8 shows that a larger value of d and a smaller inclination angle β_0 is associated with a larger Γ_3 in the 1st ASVD mode. Several singularities are noted in the 1st SVD and 1st SHC modes. Notably, with the increase in β_0, the value of d that is associated with a singularity in Γ_3 also increases.

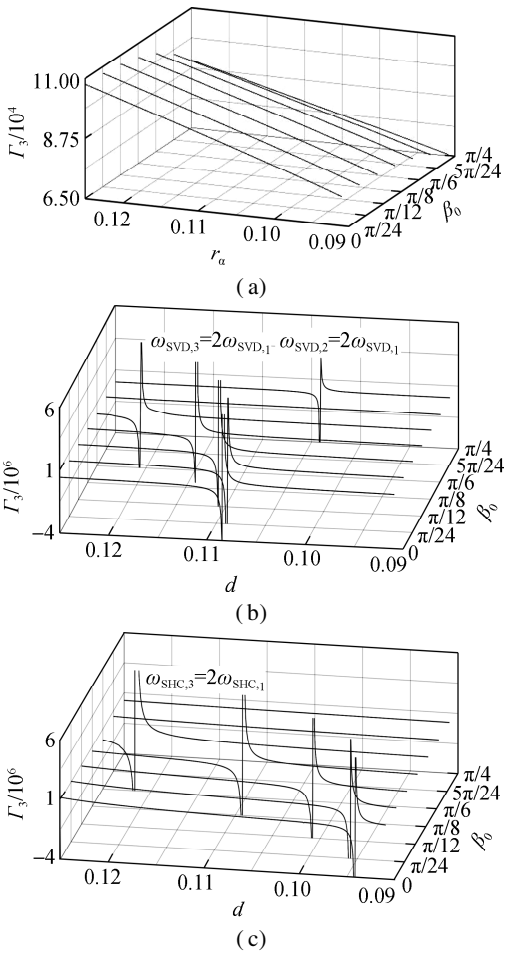

Fig. 8 Effect of d on Γ_3 for the modes when $r_\alpha = 12$. (a) 1st ASVD; (b) 1st SVD; (c) 1st SHC

Another study is conducted with the ratio r_α selected in the range of 1.0 to 16.0, and $\beta_0 \mid_{x=0,l} = (0,\ \pi/24,\ \pi/12,\ \pi/8,\ \pi/6,\ 5\pi/24,\ \pi/4)$ is adopted again. The other parameters are the same as those in Section 3. The effects of r_α on coefficient Γ_3 are depicted in Fig. 9. A general increasing trend of Γ_3 with r_α for all modes is noted. The rate of increase tends to decrease with β_0. The coefficient Γ_3 is always positive for the 1st ASVD mode with no singularity induced, which means that the 1st ASVD mode behaves as a hardening nonlinear system in all of the cases investigated. Conversely, singularities are noted in the 1st SVD and 1st SHC modes. More singularities can be induced within the same range of r_α for a larger β_0. Notably, more singularities are induced in the 1st SHC mode with an eigenfrequency ratio of 2.0 compared with the two other modes. These results indicate that a sudden change in the system properties would more likely occur in higher-order modes when r_α changes. The effects of d and r_α on Γ_2 are not investigated in this study, as they do not influence this parameter.

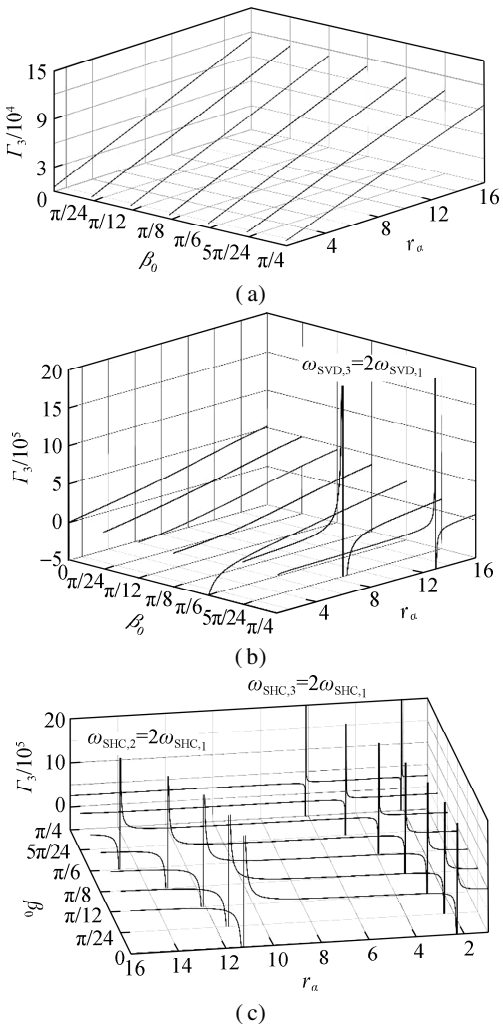

Fig. 9 Effect of r_α on Γ_3 of different modes when $d = 1/10$. (a) 1st ASVD; (b) 1st SVD; (c) 1st SHC

5 Conclusions

1) This study exhaustively conducts the parameter analysis of dynamically nonlinear properties of a suspension bridge using a continuum suspension bridge model of vertical vibrations of the bridge deck with symmetric vibration of two main cables with respect to the center line of the main girder along the spanwise direction. Different spatial inclination angles of the hanger are considered. Then, the multiple scale method is adopted to analyze the primary resonance responses of three typical vibration modes. The obtained system responses are further compared with those from the Runge-Kutta method, with good consistency indicating the accuracy of the analytical approach of nonlinear analysis.

2) Two nonlinear coefficients (i. e., Γ_2 and Γ_3) can effectively affect the nonlinear primary resonance responses of the bridge structure. The coefficient Γ_2 mainly affects the magnitude of the primary resonance response of the system and reflects system damping. The coefficient Γ_3 has a strong influence on the softening and hardening behavior of the primary resonance; hence, it is an indicator of the nonlinear stiffness of the system.

3) System parameters, such as the inclination angle of hangers, sag-to-span ratio, and tensile stiffness ratio between deck and cable, are determined to have notable influences on coefficient Γ_3. Singularities in Γ_3 can be observed in different combinations of the system parameters investigated. This singularity could cause large dramatic variations in the nonlinear dynamic properties of the system; thus, it should be avoided in the design of the bridge structure.

References

[1] Dallard P, Fitzpatrick T, Flint A, et al. London millennium bridge: Pedestrian-induced lateral vibration [J]. *Journal of Bridge Engineering*, 2001, **6**(6): 412 −417. DOI: 10.1061/(asce)1084-0702(2001)6: 6 (412).

[2] Lang T Y, Wang H, Jia H Z, et al. Vortex-induced vibration performance and wind pressure distribution of main girder of long-span suspension bridge affected by temporary facilities[J]. *Journal of Southeast University* (*Natural Science Edition*), 2022, **52**(5): 833 − 840. DOI: 10.3969/j. issn. 1001-0505. 2022. 05. 002. (in Chinese)

[3] Tao T Y, Gao W J, Jiang Z X, et al. Analysis on wind-induced vibration and its influential factors of long suspenders in the wake of bridge tower[J]. *Journal of Southeast University* (*Natural Science Edition*), 2023, **53**(6): 1065 − 1071. DOI: 10.3969/j. issn. 1001-0505. 2023. 06. 013. (in Chinese)

[4] Li Y, Yang X P, Chen Y M. Dynamic behavior analysis method for vehicle-bridge system considering abrupt cable-breakage events [J]. *Journal of Southeast University* (*Natural Science Edition*), 2023, **53**(6): 1156 − 1164. DOI: 10.3969/j. issn. 1001-0505. 2023. 06. 023. (in Chinese)

[5] Abdel-Ghaffar A M, Rubin L I. Nonlinear free vibrations of suspension bridges: Theory[J]. *Journal of Engineering Mechanics*, 1983, **109**(1): 313 − 329. DOI: 10.1061/(asce)0733-9399(1983)109: 1(313).

[6] Abdel-Ghaffar A M, Rubin L I. Nonlinear free vibrations of suspension bridges: Application[J]. *Journal of Engineering Mechanics*, 1983, **109**(1): 330 − 345. DOI: 10.1061/(asce)0733-9399(1983)109: 1(330).

[7] Çevik M, Pakdemirli M. Non-linear vibrations of suspension bridges with external excitation [J]. *International Journal of Non-linear Mechanics*, 2005, **40**(6): 901 − 923. DOI: 10.1016/j. ijnonlinmec. 2004. 11. 002.

[8] Lazer A C, McKenna P J. Large-amplitude periodic oscillations in suspension bridges: Some new connections with nonlinear analysis[J]. *SIAM Review*, 1990, **32**(4): 537 − 578. DOI: 10.1137/1032120.

[9] Ardito R, Capsoni A, Guerrieri A. Internal parametric resonance and aeroelastic effects for long-span suspension bridges[C]//*Proceedings of the 5th International Conference on Computational Methods in Structural Dynamics and Earthquake Engineering* (*COMPDYN* 2015). Crete

Island, Greece, 2015: 4508 - 4527.
[10] Capsoni A, Ardito R, Guerrieri A. Stability of dynamic response of suspension bridges[J]. *Journal of Sound and Vibration*, 2017, **393**: 285 - 307. DOI: 10.1016/j.jsv.2017.01.009.
[11] Lepidi M, Gattulli V. Non-linear interactions in the flexible multi-body dynamics of cable-supported bridge cross-sections[J]. *International Journal of Non-linear Mechanics*, 2016, **80**: 14 - 28. DOI: 10.1016/j.ijnonlinmec.2015.09.009.
[12] Peng J, Xiang M J, Wang L H, et al. Nonlinear primary resonance in vibration control of cable-stayed beam with time delay feedback[J]. *Mechanical Systems and Signal Processing*, 2020, **137**: 106488. DOI: 10.1016/j.ymssp.2019.106488.
[13] Zhang H Y, Chen Z Q, Hua X G, et al. Design and dynamic characterization of a large-scale eddy current damper with enhanced performance for vibration control[J]. *Mechanical Systems and Signal Processing*, 2020, **145**: 106879. DOI: 10.1016/j.ymssp.2020.106879.
[14] Hui Y, Kang H J, Law S S, et al. Modeling and nonlinear dynamic analysis of cable-supported bridge with inclined main cables[J]. *Engineering Structures*, 2018, **156**: 351 - 362. DOI: 10.1016/j.engstruct.2017.11.040.
[15] Hui Y, Xia C, Li K, et al. Modal characteristic and nonlinear dynamic response of suspension bridge with lateral asymmetric stiffness[J]. *International Journal of Structural Stability and Dynamics*, 2023, **23**(10): 2350110. DOI: 10.1142/s0219455423501109.
[16] Xu L, Hui Y, Yang Q S, et al. Modeling and modal analysis of suspension bridge based on continual formula method[J]. *Mechanical Systems and Signal Processing*, 2022, **162**: 107855. DOI: 10.1016/j.ymssp.2021.107855.
[17] Xu L, Hui Y, Zhu W D, et al. Three-to-one internal resonance analysis for a suspension bridge with spatial cable through a continuum model[J]. *European Journal of Mechanics—A*, 2021, **90**: 104354. DOI: 10.1016/j.euromechsol.2021.104354.
[18] Hui Y, Xu L, Jiang Y. Nonlinear torsional primary resonance analysis of suspension bridge with generalized configuration using mathematical model[J]. *Engineering Structures*, 2022, **255**: 113935. DOI: 10.1016/j.engstruct.2022.113935.
[19] Xu L, Hui Y, Liu G, et al. Internal resonance of generalized suspension bridge model considering torsional-vertical vibration[J]. *Structures*, 2023, **47**: 1754 - 1776. DOI: 10.1016/j.istruc.2022.11.131.
[20] Cao L L, Lü Y B, Cao D, et al. Influence analysis of pedestrian dynamic parameters on human-induced vibration of long span simply supported footbridge[J]. *Journal of Southeast University* (*Natural Science Edition*), 2020, **50**(2): 260 - 266. DOI: 10.3969/j.issn.1001-0505.2020.02.008. (in Chinese)
[21] Rega G, Lacarbonara W, Nayfeh A H, et al. Multiple resonances in suspended cables: Direct versus reduced-order models[J]. *International Journal of Non-linear Mechanics*, 1999, **34**(5): 901 - 924. DOI: 10.1016/s0020-7462(98)00065-1.
[22] Nayfeh A H, Mook D T. *Nonlinear oscillations*[M]. Weinheim, German: John Wiley & Sons, 2008: 127 - 128.
[23] Cheng P, Kang H J. Modeling and analysis of 1∶3 internal resonance of suspension bridge under boundary excitations[J]. *International Journal of Structural Stability and Dynamics*, 2024: 2550005. DOI: 10.1142/s0219455425500051.
[24] Nayfeh A H, Balachandran B. *Applied nonlinear dynamics*: *Analytical, computational, and experimental methods*[M]. New York: Wiley, 1995: 432 - 434.
[25] Xu L, Hui Y, Li K. Non-linear dynamic analysis on a continuum suspension bridge model with spatial layout of main cables[J]. *International Journal of Structural Stability and Dynamics*, 2022, **22**(7): 2250041. DOI: 10.1142/s0219455422500419.
[26] Lacarbonara W, Paolone A, Vestroni F. Non-linear modal properties of non-shallow cables[J]. *International Journal of Non-linear Mechanics*, 2007, **42**(3): 542 - 554. DOI: 10.1016/j.ijnonlinmec.2007.02.013.

空间索面悬索桥的非线性主共振参数分析

回 忆[1] 徐 亮[2]

([1] 重庆大学土木工程学院, 重庆 400030)
([2] 苏州科技大学土木工程学院, 苏州 215011)

摘要:针对空间索面悬索桥的非线性振动问题,采用一种基于连续介质理论的广义模型开展了非线性主共振参数分析. 该模型同时考虑了悬索桥的桥面竖向运动和缆索竖向-水平运动的几何非线性特点. 基于该模型和时间多尺度法,推导了求解空间索面悬索桥的竖弯模态主共振响应的调制方程. 研究表明,调制方程中的非线性系数会显著影响系统主共振的最大响应幅值,并影响竖弯振动模态的硬化或软化特性. 此外,主缆与吊杆的倾角、主缆垂跨比、主梁与主缆的抗拉刚度比等系统参数对非线性系数同样存在显著影响,特别是当系统参数位于奇异点附近时,系统的动力特性会随梁体和主缆的对称振动模态对应的非线性系数突变而剧烈变化,在系统设计中应避免这种情况. 该研究能够为该类桥梁的结构设计提供参考.

关键词:悬索桥;空间主缆;非线性动力学;时间多尺度法;主共振
中图分类号:U441.3